Proceeding of the 14th International Forum of Automotive Traffic Safety, 2017, pp 519-529
No.ATS.2017.514

Development and Validation of a Mixed Mid-sized Human Body FE Model in Rear-end Collision

Fan LI[1], Ronggui LU[2]
State key Laboratory of Advanced Design Manufacturing for Vehicle Body
Hunan University, Changsha 410082, China

Email:lifandudu@163.com

Abstracts: Although human body finite models (HBM) are employed widely in studies on occupant damages in vehicle crash, the current models are not meticulous enough to perform researches, most of which contains no brain structure or spinal cord parts. Hence the focus of this paper was to develop a mixed mid-sized human body FE model including the validated HBM-head with brain structures, the newly built spinal cord with gray matter, white matter, dura and pia part, the hybrid Ⅲ dummy without the head-neck part, the sled constraint system. The validation of the HBM-head model can refer to the study of JK Yang et al. The spinal cord was validated against published literatures under static uniaxial tension, compression as well as impact experiment and integrated into the brain stem of HBM-head model with joint nodes. The mixed HBM was then restricted in sled constraint system to verify its effectiveness against the volunteer experiments results. The outcomes confirmed that the mixed HBM had good biofidelity and could be used to further study the underlying mechanisms of occupant injuries in vehicle collisions.
Keywords: HBM; Spinal cord; rear-end collision; Occupant

1 Introduction

According to the report of WHO[1], the figure of people killed in road traffic accidents were 1.4 million in 2002 which was projected to almost double in 2020. Occupant's injuries resulted from vehicle crash were especially severe and the number of accidents ranked the second largest behind the pedestrian damages [2].

To study the injury mechanism, animal tests [3-5] and cadaver studies [6-8] were utilized at early stage, which caused the ethic problems. So multi-rigid models were then constructed [9] that was found fail to measure the stress and strain distribution of tissues and model the compression stiffness and friction. Since then, many finite models have been developed as an effective tool as the considerably improvement of computational techniques. Standardized crash dummy model were framed using the past calculation codes [10-11]. Although they possessed undeniable qualities, they suffer from the defects of their physical counterparts, especially the limited biofidelity. In 1998, a seated 50th percentile adult male finite model was developed with the explicit Radioss code. However, parts of its head, lower and upper extremity were not meticulous enough. It was only a kinematic model reproducing physical quantities such as forces, deflections and accelerations. The HUMOS model, established in the context of a European collaboration [12, 15], was from sections of a cadaver frozen in a seated driver occupant position. And the poor biofidelity may result from failure properties of biological tissues and blood pressure effects. The THUMS model, a mid-size adult occupant, was developed in order to estimate overall injuries in traffic accident situations. Each part of the model such as the head, neck and thorax, were validated in more than one impact situation, while the face, shoulder, and internal organs were only validated in one impact situation. Also the models of the internal brain structures meshed with eight-node solid element were not lifelike enough [13]. In 2003, the SIMON model, whose structures were considered as deformable, linear viscoelastic, isotropic, and homogeneous, was developed. However, the skull was assumed rigid that failed to study skull fracture [17]. The global human body model (GHBM), developed by Gayzik et al, including models of head, neck, abdomen and other parts. While the hyoid bone was modeled as a rigid body, the falx was modeled with shell elements instead of solid ones [18].

Unlike the HBM models mentioned above, the mixed HBM developed in this study contained high biofidelity, the reconstruction of the spinal cord model was originated from volunteer sitting in a driving state, which avoided the defects brought by the cadaver. Many part such as the head and neck were well validated through different impact simulations [35, 36] and the falx part within the brain was modeled with solid eight-node element instead of shell. The skull was also improved with rigid material changed into deformable. In this paper, the rigid head of the New HBM Head-Neck FE model validated by Li et al [26, 35] was replaced with HBM-head model consisting of detailed brain structures that was validated by JK Yang et al [14]. The Changed New HBM Head-Neck FE model and the hybrid III dummy model without head-neck part were integrated with one-dimensional beam elements and nodal connections as well as surface-surface contacts. Then the mixed dummy FE model was positioned in the sled constraints systems and validated by comparing with the published experimental data obtained from rear-end volunteer tests conducted by Davidsson et al [16].

2 Methods and materials

2.1 FE Model Construction

The head part of New HBM Head-Neck FE model was modeled with rigid shell elements, leading to the in-capability in researching the brain damages resulted from vehicle crashes [35]. In this paper, the head was replaced by the HBM-head model (Fig. 1) validated by JK Yang et al. The effectiveness was validated against the results from the Nahum's impact experiment using human head specimen. The sensitivity and biofidelity of the FE model for predicting brain traffic injury were detected through parameter analysis at different impact speeds [14].

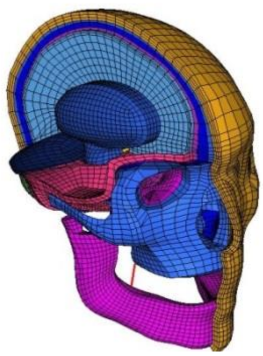

Figure 1. HBM-head model, referring to study[14]

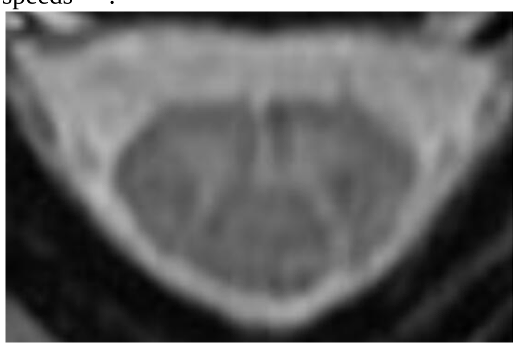

Figure 2. MRI image of the spinal cord

The MRI cross section images of the spinal cord of a healthy younger volunteer, scanned from CT (Fig. 2), were used to obtain the outlines of gray matter and white matter with Mimics 14.0 software. The outlines were then imported into HYPERMESH 13.0 software creating the responded areas that were then stretched to be a 3D geometry. For simplify, the geometry was assumed to be symmetrical about the mid-sagittal plane. Thus half of the spinal cord was reconstructed at first and the whole model was then integrated by reflection.

The geometry of the dura, followed the inner contour of spine canal, was modeled with shell elements with the thickness set to 0.1mm. A layer of shell element with thickness of 0.1 mm was generated on the outer surface of white matter, representing the structure of pia according to the published literature [20]. The white matter and grey matter as well as cerebrospinal fluid (CSF) were all meshed with eight-node solid element (Fig 3)

The finite model included gray matter, white mater, dura and pia as well as CSF. Piecewise linear plasticity material properties were assigned to the dura, pia, white matter and gray matter except the CSF tissue that was applied with visco-elastic material [21-27].

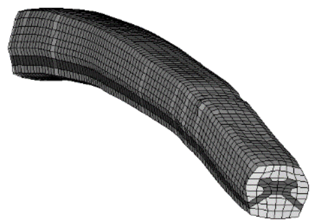

(1) the white and gray model

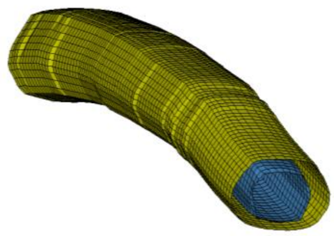

(2) The dura and pia model

(3) The CSF model

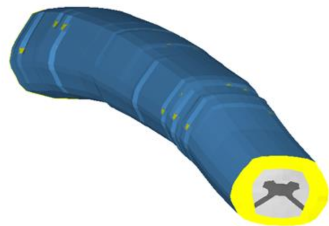

(4) The whole spinal cord model

Figure 3. The spinal cord model

The stress-strain curves of the materials were shown in figure 4. Other parameters of materials were illustrated on the table 1 below.

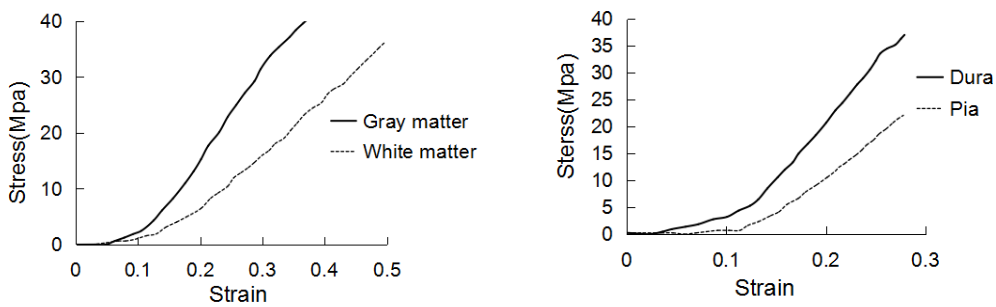

Figure 4. Stress-Strain curves of pia and dura, gray and white maters, , referring to [21-27]

Table 1. Mechanical properties of materials applied in spinal cord, referring to study [21-27]

Tissues	E (Pa)	Material type	μ	Density (KG/m^3)	Mechanical property
White matter	2.77E5	Piecewise linear plasticity	0.4	1050	Seen figure 4
Gray matter	6.56E5	Piecewise linear plasticity	0.4	1050	Seen figure 4
Dura	3.15E7	Piecewise linear plasticity	0.45	1140	Seen figure 4
pia	2.3E6	Piecewise linear plasticity	0.45	1140	Seen figure 4
CSF	--	visco-elastic	--	1040	BULK=2190MPa G0=1.0 KPa G∞=0.9 KPa β=80 s-1

The spinal cord model was well placed into the neck model with contact definition defined. Many spotwelds element were used to help support its position and make sure the distance related to the ligaments. On the one hand, the HBM-head model was linked to the neck with beam and discrete elements, on the other hand, the spinal cord including dura, pia, gray matter and white matter were connected to the stem with shared nodes. The Changed New HBM Head-Neck FE model and its detailed inner structure were as shown in figure 5.

Figure 5. the Changed New HBM Head-Neck FE model

Hybrid III dummy was developed by General Motors in 1976 and was widely used in vehicles companies. Its FE counterpart can be mainly divided into head, neck, chest, abdomen, pelvis and limbs, which consists of 148 parts, containing a total of 4412 elements and 7784 nodes (figure 6).

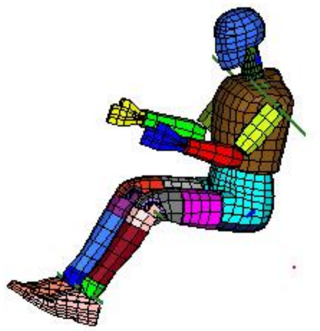

Figure 6. Hybrid III dummy

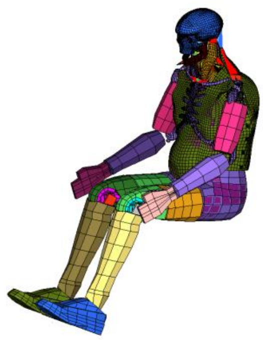

Figure 7. Mixed-dummy Human Body FE Model

In the HYPERWORKS software, first the head-neck part of the Hybrid III dummy was removed and the rest part was taken as the base for the Changed New HBM Head-Neck FE model that was connected to the first thoracic T1 of Hybrid III dummy with CONSTRAINED_EXTRA_NODES_SET. The connection between thorax of the Changed New HBM Head-Neck FE model and the base of Hybrid III dummy was realized through CONSTRAINED_RIGID_BODIES. In order to eliminate the impact of the thorax during the simulation, the density of that was minimized and its contact with the Hybrid III dummy was not defined (figure 7).

The constraint system, including seat, seatbelt, rigid front floor and pedal, was well matched as was shown in figure 8. The retractor, sliprings, 1D and 2D seatbelt elements were realized in the seatbelt whose belt routing was defined according the mixed dummy. The mixed dummy model was then set into the constraint system and contacts among the dummy, the seat and the seatbelt were defined by CONTACT_AUTOMATIC_SURFACE_TO _SURFACE in HYPERMESH. The integrated complex dummy model was shown in Figure 9.

2.2 FE model validation

Spinal cord validation

The spinal cord model needed to be validated against the animal experiments, which would ensure the effectiveness of its proper mechanics properties. To validate the model, one single cross section area was chosen and stretched to 150mm to develop the simplified model [28]. The simplified spinal cord model, without dura mater, pia matter and CSF matter, was loaded under uniaxial tension [29] and posterior compression [37] as well as the impact simulation [32]. The computed elongation-force curve in uniaxial direction and reduction-force curve in posterior direction as well as the stress distribution counter was compared with the published experimental results.

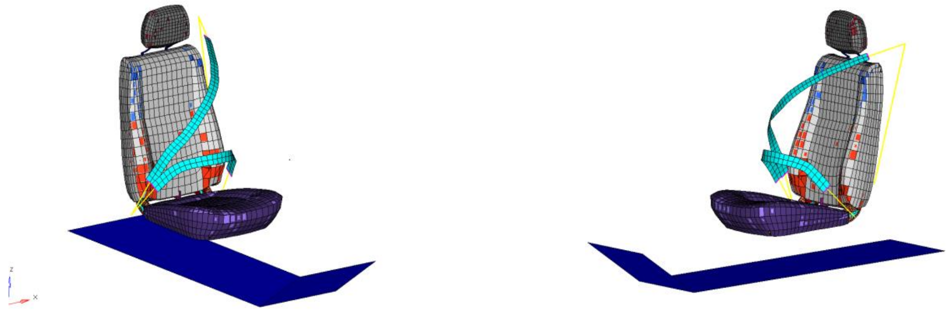

Figure 8. The constraint system

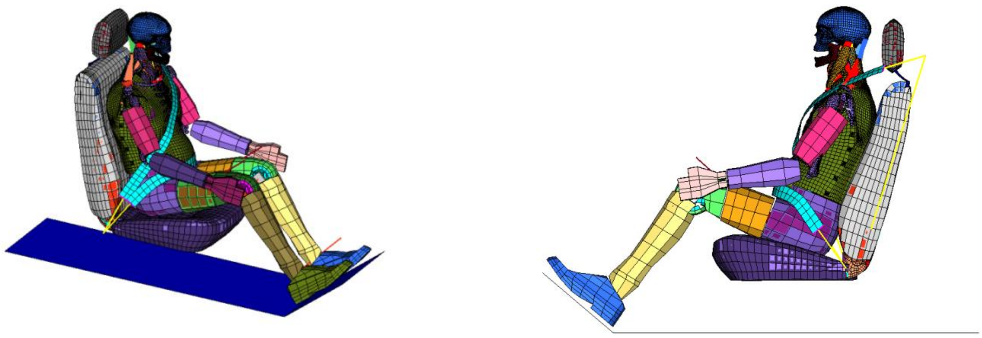

Figure 9. The complex dummy model for validation

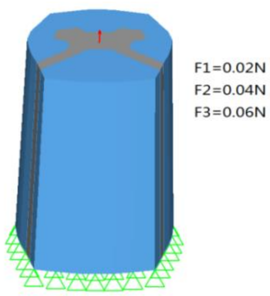

Figure 10. Uniaxial stretch simulation

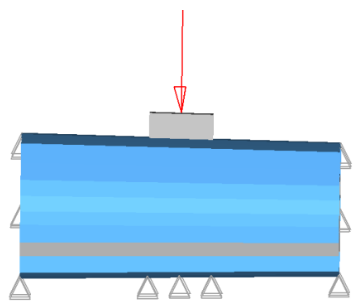

Figure 11. Static compression validation

The boundary and loading condition in the FE model were adopted from an in vitro experiment [29] in the uniaxial tension simulation. All the nodes at caudal end of the spinal cord model were fully constrained in all directions and all the nodes at cephalic end were constrained in all the directions except the stretching z axis [28,31] (Figure 10). The absolute magnitudes of the axial force applied in the model were 0.02, 0.04, and 0.06 N, respectively [28].

In the posterior compression verification (Figure 11), all the nodes in both caudal and cephalic ends of the spinal cord model were fully constrained. To represent the fixed posterior surfaces of the cervical cord, the ventral surface of the spinal cord model was fixed [31]. According to the study of Raynor and Kingman et al[30], the region of the middle third of the spinal cord model was applied the loads of 0.01, 0.02, 0.03, 0.04, 0.05 N along the negative y axis with a flat contact area, respectively.

An impact experiment of rat spinal cord was performed by Cao Y et al [32] to find out the injury condition of spinal cord. To ensure the force to be distributed evenly, a 3mm×3mm washer was placed right on the impact position. The 8g strike stick was freed from a height of 4cm and hit the T10 level of spinal cord. The damage was then observed through CT scanner and optical microscope images. In the impact simulation, since the diameter of human spinal cord was about

12mm, a 10mm×10mm washer was used. The mass of the strike stick was set 89g and the free-fall height was set 4cm, making sure the consistency of the unit force between the experiment and the simulation (Figure 12). The stress counter was finally photographed to find out the damage condition.

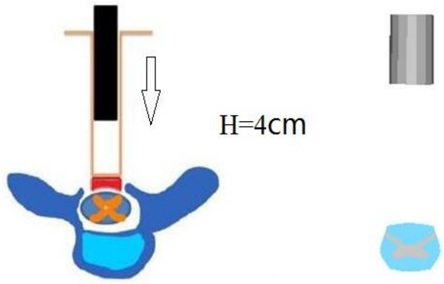

Figure 12. Impact validation

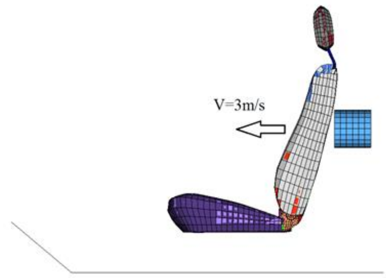

Figure 13. Seat validation

Seat validation

The effectiveness of the seat was well validated through pendulum impact (Figure 13). The pendulum model, a cylinder with radium set to 152.4mm and mass set to 23.4kg, was constrained in all directions except the z degree of freedom with impact velocity set to 3m/s. The acceleration of the pendulum centroid was documented and compared with seat impact experiment.

Mixed HBM validation

The effectiveness of the mixed dummy in rear-end collision was validated by performing the simulation referring to the volunteer experiment conducted by Davidsson et al [16]. In the experiment, eleven male volunteers, without prior history of cervical spine injury, participated in a total of 23 rear-impact tests. The volunteers were seated in either a laboratory seat or a standard seat mounted on a target sled and restrained by a lap and a shoulder belt. They were instructed to place their hands on the side of their thighs and position their feet on an angled plate as well as holding their heads leveled and relaxed (Figure 14). A bullet sled (570 kg) then hit the stationary target sled (890 kg excluding volunteer) which was then accelerated forward. The sled acceleration (Figure 15) and the kinematic responses corridors of the head were documented.

In the simulation, the front floor and the pedal was modeled with simplified rigid elements and the acceleration resulted from volunteer experiment was applied to a node of the element. The kinematic responses including the horizontal displacement, the horizontal acceleration and the head angle documented from the simulation were compared with the corridors from the experiment.

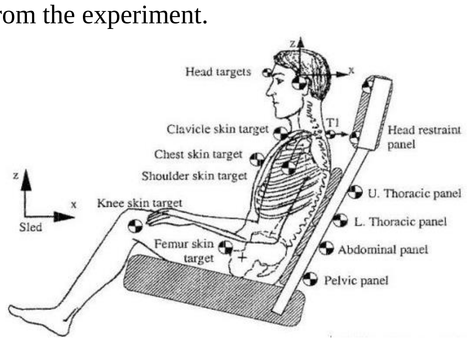

Figure 14. Side-view of volunteer seat position, referring to study [16]

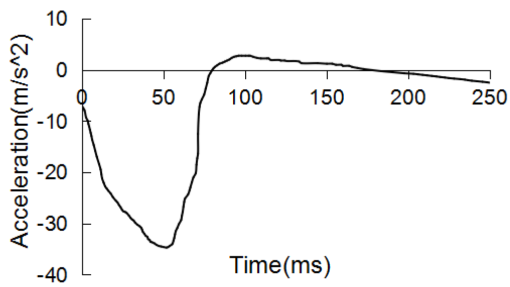

Figure 15. The sled acceleration, referring to study [16]

3 Results

3.1 Spinal cord validation result

Figure 16 showed that the relationship of the distraction force and the change in length of the spinal cord in the tension study shared the same trend with that from the in vivo experimental [29]. Compared to the published in vivo static compression experiment [30], the curve of compression forces and deformation in the posterior-anterior direction showed non-linear trend that was similar to the experimental results. Although the result showed poor linear behavior compared with Xin Feng et al's study [28], they all shared the the same trend (Figure 17).

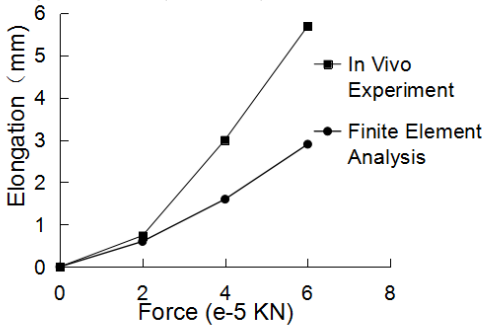

Figure 16. Uniaxial stretch simulation

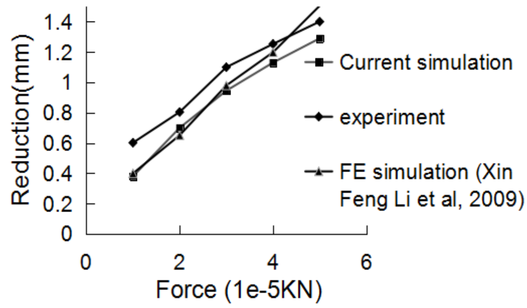

Figure 17. Static compression validation

The CT and optical microscope images before and after the striking were shown in Figure 18, which clearly showed that the blood vessels in the central region suffer serious injury while the vessels in the surrounding area were rarely damaged [32]. The stress counter from the simulation showed that the stress in the center area (gray matter) was higher than that in the surrounding area (white matter). The injury potential was consistency with the experiment result.

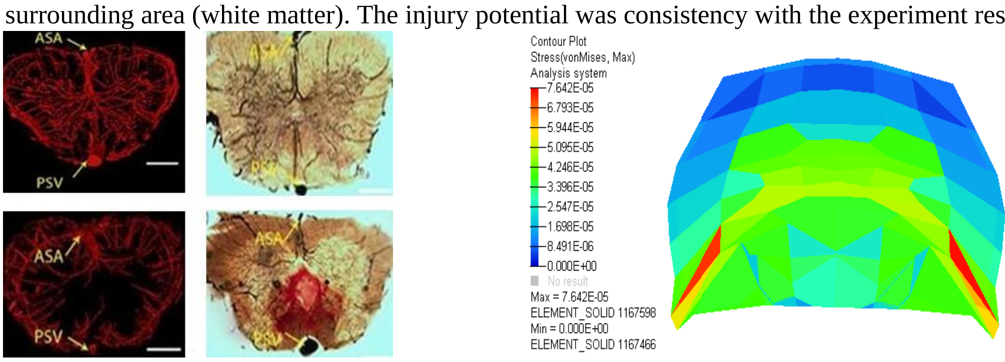

Figure 18. The left were CT and optical microscope images [32], the right were the stress distribution counter.

3.2 Seat validation result

The acceleration curves resulted from the simulation and experiment, illustrated in figure 19, contained high consistency, which verified the effectiveness of the seat.

The overall dynamic responses of the rear-end crash model from 0ms to 250ms were shown in figure 20. During the time between 0ms and 70ms, the model was in a static equilibrium state. Beyond this period the thorax was pushed by the seat and T1 began to drive the cervical vertebra C2-C7 moving forward. Because of inertia, the head had no

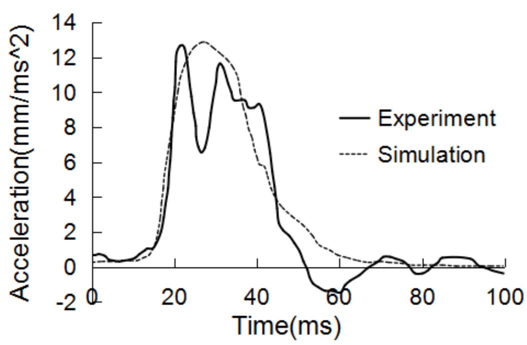

Figure 19. Validation of the seat

3.3 Mixed HBM validation result

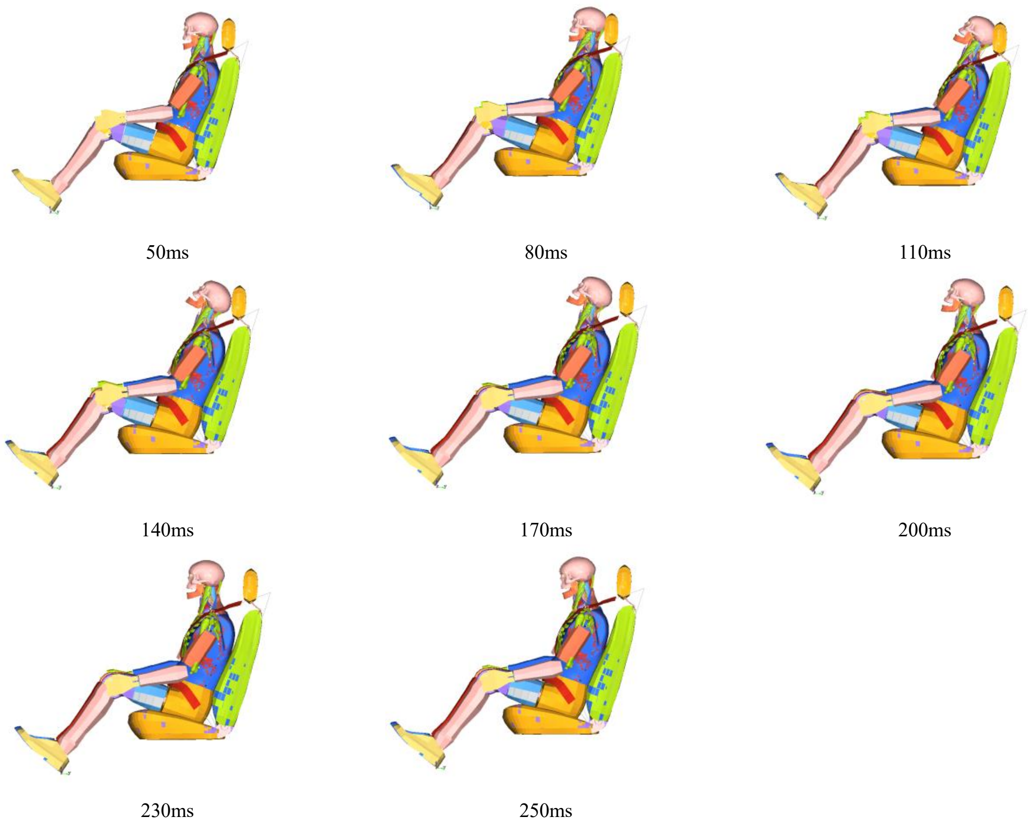

Figure 20. The dynamic responses of the mixed dummy FE model

Movement with respect to the initial space until 75ms. From 75ms to 110ms, the head was lowering down to the headrest and the whole cervical spine was in an obvious extended state. The head continued to turn down until the head reached its maximum rotation angle at 168ms when the cervical spine appeared in a compression-bending-shear state. During the time between 168ms and 250ms, the head gradually rebounded under the traction of the neck and the push of the headrest.

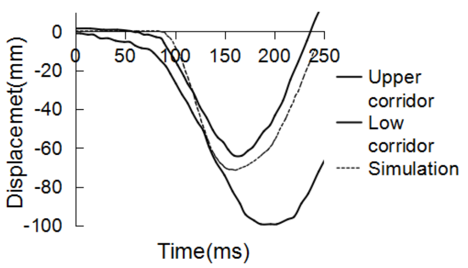

A

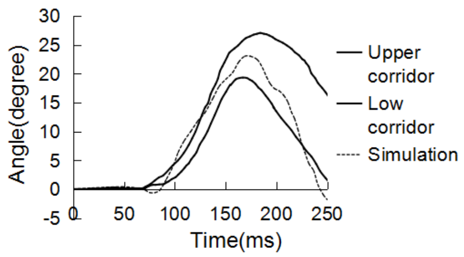

B

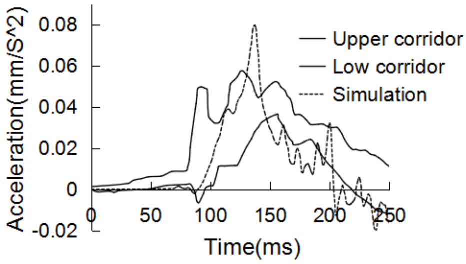

C

Figure 21. Head x displacement (A), Head angle (B), Head x acceleration (C)

From the curves in Figure 21, the responses of the head were consistent with the experimental corridors. With respect to the head x displacement, most part of the curve were within the corridor and the time when the head began to low down was only a little later. The trends of the displacement resulted from the experiment and simulation were exactly the same. As far as the head angle was concerned, nearly 90% of the curve was within the experiment corridor. The maximum angle of the head centroid in the simulation fell between that of the upper and low corridors. The curve shared the same trend with the experiment result, which was similar to the head x displacement. As to the head x acceleration, the curve documented from the simulation from 0ms to 130ms were within the corridor and behaved the same trend compared with corridors, while the maximum value was beyond the experimental upper limit by about 38%. From 140ms, although the curve contained fluctuation, the overall trend was the same with the experimental corridors.

4 Discussion

In this study, the mixed 50th dummy FE model was successfully constructed and validated. It included the validated HBM-head with brain structure, the newly built spinal cord, hybrid III dummy without the head model, the sled constraint system. Firstly the spinal cord was validated against published literatures under static uniaxial tension with 0.02, 0.04, and 0.06 N applied in the uniaxial direction, respectively, compression with 0.01, 0.02, 0.03, 0.04, 0.05 N along the negative y axis respectively as well as impact experiment with 89g strike stick impacting the spinal cord from a height of 4cm. Then in order to verify the biofidelity of the mixed dummy model against the experiments corridor, the model was restricted in sled systems and loaded by the pulse referring to the sled volunteer experiment. The results confirmed that the responses contained consistency comparing to the experiment data, which suggested the good biofidelity of the mixed dummy model and it could be used to further study the underlying injury mechanisms of occupant injuries in vehicle collisions.

The reconstruction of the 3D spinal model included many simplifications regarding the geometry, materials, and interactions between components, which contained some shortcomings. The geometry of the spinal cord was reconstructed by stretching the cross images along z axis, which may easily ignore the real detailed features that possibly affecting the behavior in the validations. In order to develop good connection between brain stem and spinal cord, a method of using joint nodes was used to make sure the connectivity, which needed the spinal cord to be meshed with eight-node element as developing the brain stem, instead of six-node solid element. This may further make many small features of the geometry eliminated. Since the shape of the CSF was difficult to measure [30], it was created based on making sure the smooth of the spinal cord model. Because there existed no consensus on the material properties of the spinal cord [21-27, 34], the material properties were adopted from published results in studies [21-27]. The detailed tissues between the spinal cord and cervical vertebras were not modeled and the interactions within them were simplified through setting the contacts and many spotwelds connecting the longitudinal ligaments and the spinal cord, the spinal cord and the cervical vertebras in both caudal and cephalic ends.

The validation results of the spinal cord were in good agreement with that from the published literatures. The change in length-force curves both in uniaxial tension and posterior compression studies behaved nonlinear and share the same trend with the responded experiment results. In the impact simulation, the stress distribution of the cross section image was well related with the CT and optical microscope images from Cao Y et al's experiment [32]. The equivalent method of applying 89g strike stick in the impact simulation instead of 8g strike stick in the rat spinal cord in the experiment [32] was an effective way to form the relationship between human and animal spinal cord study.

As to the mixed FE dummy model, its dynamic responses showed good consistency with the sled volunteer experiments (figure 21) and the biofidelity is within our anticipation. However, the head x acceleration contained obviously fluctuation in the later period when the head was rebounding. It was assumed that this phenomenon may result from the simplification of the tendons connecting to the head and the cervical vertebras, the intervertebral discs, the gaps among neck muscles as well as the lack of preload to the soft tissues. And in our future study, the complexity of the model needed to be increased.

This paper successfully developed a 50th mixed FE dummy model with its bifidelity validated in rear-end crash. The model can be utilized in the future study on the occupant injury mechanism.

5 Reference

[1] Peden, M., Scurfield, R., Sleet, D., Mohan, D., Hyder, A. A., & Jarawan, E., et al. (2005). World report on road traffic injury. Medical Journal Armed Forces India, 61(1), 255.

[2] Odero, W., Garner, P., & Zwi, A. (1997). Road traffic injuries in developing countries: a comprehensive review of epidemiological studies. Tropical Medicine & International Health Tm & Ih, 2(5), 445.

[3] Meaney, D.F, Smith, D., Ross, D.T., and Gennarelli, T.A. (1993). Diffuse axonal injury in the miniature pig: Biomechanical development and injury threshold. ASME Crashworthiness and occupant protection in transportation systems 25: 169-175.

[4] Gennarelli, T.A., Thibault, L.E., Adams, J.H., Graham, D.I., Thompson, C.J., and Marcincin, R.P. (1982a) Diffuse axonal injury and traumatic coma in the primate. Annals of Neurology 12(6): 564-574.

[5] Stalnaker, R.L., Alem, N.M., Benson, J.B., Melvin, J.W. (1977) Validation studies for head impact injury model. Final report DOT HS-802 566. National Highway Traffic Safety Administration, U.S., Department of Transportation, Washington, DC.

[6] Hodgson VR, Gurdjian ES, Thomas LM. (1966) Experimental skull deformation and brain displacement demonstrated by flash x-ray technique. Journal of Neurosurgery. Nov 25(5):549-52.

[7] Yoganandan, N., Pintar FA, Sances A Jr, Walsh PR, Ewing CL, Thomas DJ, Snyder RG. (1995) Biomechanics of skull fracture. Journal of Neurotrauma. Aug. 12(4):659-68.

[8] Hardy, W.N., Foster, C., Mason, M., Yang, K., King, A., Tashman, S. (2001) Investigation of head injury mechanisms using neutral density technology and high-speed biplanar X-ray. Stapp Car Crash Journal 45: 337-368.

[9] Mkj, J. D., Sauren, A., Thunnissen, J., & Wismans, J. (1996). A global and a detailed mathematical model for head-neck dynamics.

[10] Midoun, D. E., Abramoski, E., Rao, M. K., & Kalidindi, R. (1993). Development of a Finite Element Based Model of the Side Impact Dummy. International Congress & Exposition.

[11] Fountain M., Happee R., Wismans J., Lupker H. and Koppens W. (1996). Hybrid Modeling of Crash Dummies for Numerical Simulation proceeding of IRCOBI conference, pp401-420

[12] Thollon, L., Arnoux, P. J., Kayvantash, K., Cavallero, C., & Brunet, C. (2002). Human injury evaluation using humos radioss finite element model. PROCEEDINGS OF THE INTERNATIONAL IRCOBI CONFERENCE.

[13] Iwamoto, M., Kisanuki, Y., Watanabe, I., Furusu, K., Miki, K., & Hasegawa, J. (2002). Development of a finite element model of the total human model for safety (THUMS) and application to injury reconstruction. Proceedings of the 2002 International Research Council on Biomechanics of Injury, Munich, Germany, 31-42.

[14] Yang, J. K., Yong, P., & Wei, X. (2009). Establishment of a head finite element model of craniocerebral trauma and model validation. Journal of Clinical Rehabilitative Tissue Engineering Research, 13(52), 10391-10396.

[15] Robin, S. (2001). Humos: human model for safety - a joint effort towards the development of refined human-like car occupant models.

[16] JOHAN DAVIDSSON, CHRISTIAN DEUTSCHER, WOLFRAM HELL, PER LÖVSUND, & MATS Y. SVENSSON. (2001). Human volunteer kinematics in rear-end sled collisions. Journal of Crash Prevention & Injury Control, 2(4), 319-333.

[17] Takhounts, E. G., Eppinger, R. H., Campbell, J. Q., Tannous, R. E., Power, E. D., & Shook, L. S. (2003). On the development of the simon finite element head model. Stapp Car Crash Journal, 47(47), 107.

[18] Gayzik, F. S., Moreno, D. P., Vavalle, N. A., Rhyne, A. C., & Stitzel, J. D. (2012). Development of the global human body models consortium mid-sized male full body model. Injury Biomechanics Research. In Proceedings of the 39th International Workshop.

[19] Feller, L., Kleinbach, C., Fehr, J., & Schmitt, S. (2016). Incorporating Muscle Activation Dynamics into the Global Human Body Model. In IRCOBI Conference Proceedings.

[20] Ozawa H, Matsumoto T, Ohashi T, Sato M, Kokubun S (2004) Mechanical properties and function of the spinal pia mater. J Neurosurg Spine 1: 122–127.

[21] Ichihara, K., Taguchi, T., Shimada, Y., Sakuramoto, I., Kawano, S., & Kawai, S. (2001). Gray matter of the bovine cervical spinal cord is mechanically more rigid and fragile than the white matter. Journal of neurotrauma, 18(3), 361-367.

[22] Khuyagbaatar, B., Kim, K., & Kim, Y. H. (2014). Effect of bone fragment impact velocity on biomechanical parameters related to spinal cord injury: a finite element study. Journal of biomechanics, 47(11), 2820-2825.

[23] Roth, S., Raul, J. S., & Willinger, R. (2008). Biofidelic child head FE model to simulate real world trauma. Computer methods and programs in biomedicine, 90(3), 262-274.

[24] Zhou C，Khalil T B，King A I，et al. (1997) Head injury assessment of a real world crash by finite element modeling [J]. NASA， .

[25] Willinger, R., Taleb, L., & Kopp, C. M. (1995). Modal and temporal analysis of head mathematical models. Journal of Neurotrauma, 12(4), 743.

[26] Li, F., Laville, A., Bonneau, D., Laporte, S., & Skalli, W. (2014). Study on cervical muscle volume by means of three-dimensional reconstruction. Journal of Magnetic Resonance Imaging, 39(6), 1411-1416.

[27] Czyż, M., Scigała, K., Jarmundowicz, W., & Będziński, R. (2011). Numerical model of the human cervical spinal cord--the development and validation. Acta of Bioengineering & Biomechanics, 13(4), 51-58.

[28] Li, X. F., & Dai, L. Y. (2009). Three-dimensional finite element model of the cervical spinal cord: preliminary results of injury mechanism analysis. Spine, 34(11), 1140-1147.

[29] Maiman, D. J., Coats, J., & Myklebust, J. B. (1989). Cord/spine motion in experimental spinal cord injury. Journal of Spinal Disorders, 2(1), 14-9.

[30] Raynor RB, Kingman AF. (1968). Cervical spine injuries. J Trauma; 8:597–604.

[31] Yan, Y. B., Wei, Q., Wu, Z. X., Qiu, T. X., Ee-Chon, T., & Wei, L. (2012). Correction: finite element study of the mechanical response in spinal cord during the thoracolumbar burst fracture. Plos One, 7(9), e41397.

[32] Cao, Y., Wu, T., Yuan, Z., Li, D., Ni, S., & Hu, J., et al. (2015). Three-dimensional imaging of microvasculature in the rat spinal cord following injury. Scientific Reports, 5, 12643.

[33] Tencer AF, Allen BL Jr, Ferguson RL (1985) A biomechanical study of thoracolumbar spine fractures with bone in the canal. Part III. Mechanical properties of the dura and its tethering ligaments. Spine (Phila Pa 1976) 10: 741–747.

[34] Sparrey, C. J., Manley, G. T., & Keaveny, T. M. (2009). Effects of white, grey, and pia mater properties on tissue level stresses and strains in the compressed spinal cord. J Neurotrauma, 26(4), 585-595.

[35] Rong Gui Lu., Fan Li. (2016) Development and Validation of a Neck Muscle FE Model for Lateral Impact Simulation, Proceeding of the 13th international forum of automotive traffic safety, 531-543.

[36] Fan, L. I., Cao, Y. C., Si-Cheng, S. U., & Jing, H. (2016). Development and validation of a neck muscle fe model for rear impact study. Journal of Hunan University.

[37] Hung, T. K., Lin, H. S., Bunegin, L., & Albin, M. S. (1982). Mechanical and neurological response of cat spinal cord under static loading. Surgical neurology, 17(3), 213-217.